Biosensors

DOI: 10.1002/anie.200800382

Temperature-Controlled Molecular Depolarization Gates in Nuclear Magnetic Resonance**

Leif Schröder, Lana Chavez, Tyler Meldrum, Monica Smith, Thomas J. Lowery, David E. Wemmer, and Alexander Pines*

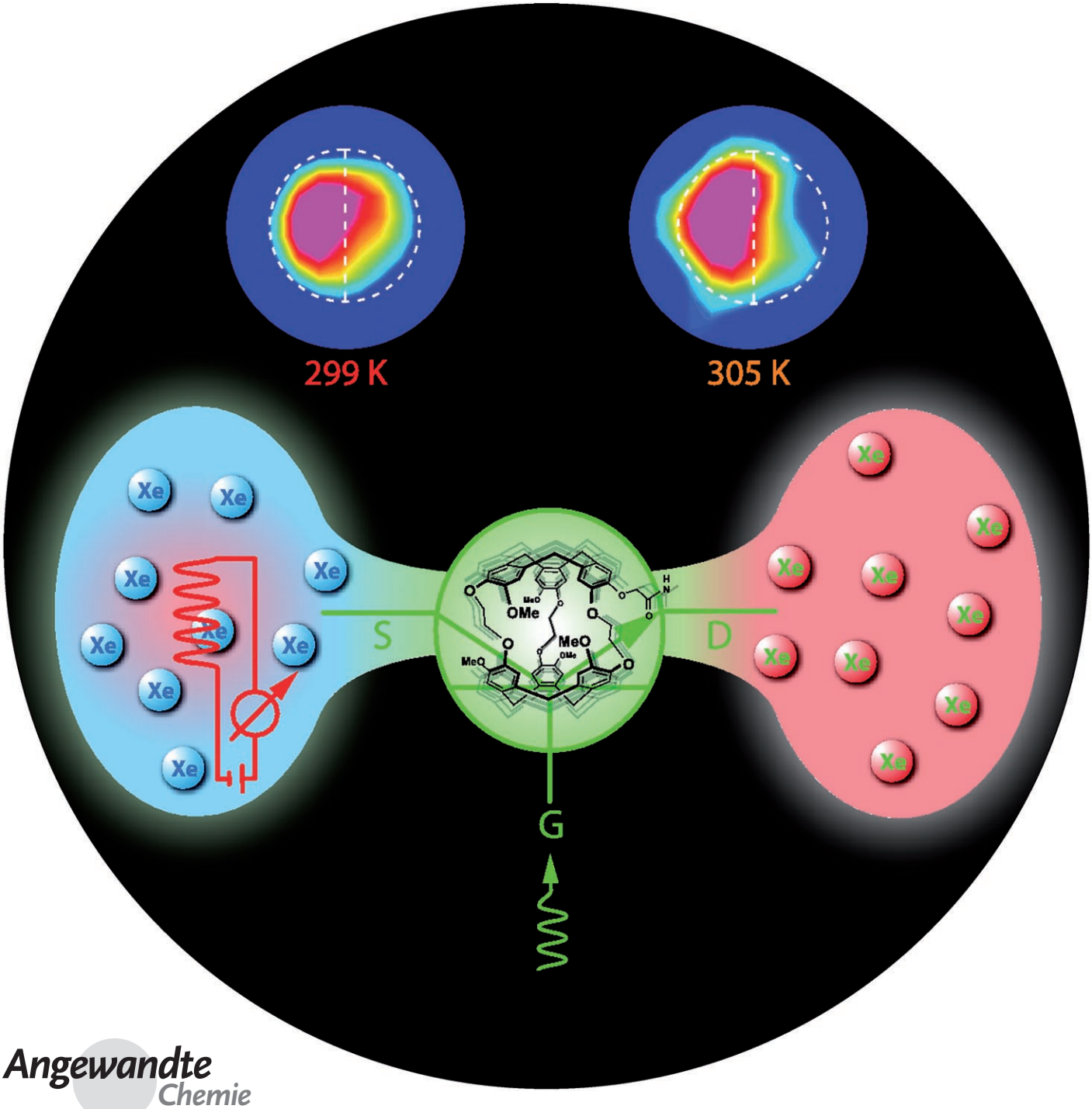

The potential of nuclear magnetic resonance (NMR) to yield spectroscopic and imaging (MRI) information based on molecule-specific signals is often impeded by its intrinsic low detection sensitivity. Amplifying the available magnetization has been the focus of many studies, leading to various hyperpolarization (hp) techniques, such as hp noble gases,[1,2] parahydrogen-induced polarization transfer,[3,4] or dynamic nuclear polarization.[5] Exploiting chemical exchange of nuclei of a hyperpolarized reservoir in combination with a mechanism of gated transfer onto the molecule of interest would provide optimized, controlled utilization of the hyperpolarization (Figure 1 a), thus avoiding polarization losses during transfer reactions. As exchange rates depend on the ambient temperature, the amplification achieved by transferring information from a low-concentration target pool onto the high-concentration reservoir pool can be tuned. Herein, we demonstrate the implementation of this concept using molecular cages to host hp xenon, and apply this approach to noninvasive molecular temperature sensing.

Cryptophane cages temporarily encapsulate xenon[6] and facilitate functionalized molecular biosensors that combine high specificity in detecting biomolecules and high sensitivity of hp ^{129}Xe.[7] The spins of bound nuclei can be selectively depolarized with radio-frequency pulses because of the unique chemical environment offered by the cage. Subsequent release into the bulk pool decreases the net magnetization in the surrounding medium. The Hyper-CEST technique allows for efficient depolarization transfer[8] by using continuous wave (cw) irradiation for a few seconds, leading to saturation of the caged spin ensemble.

[*] Dr. L. Schröder, Dr. L. Chavez, T. Meldrum, Prof. A. Pines
Lawrence Berkeley National Laboratory
Materials Sciences Division
and
University of California Berkeley, Department of Chemistry
Berkeley CA 94720 (USA)
Fax: (+1) 510-486-5744
E-mail: LSchroeder@lbl.gov
Pines@berkeley.edu
M. Smith
Lawrence Berkeley National Laboratory
Physical Biosciences Division
and
University of California Berkeley, Biophysics Graduate Group
Berkeley CA 94720 (USA)
Dr. T. J. Lowery,[+] Prof. D. E. Wemmer
Lawrence Berkeley National Laboratory
Physical Biosciences Division
and
University of California Berkeley, Department of Chemistry
Berkeley CA 94720 (USA)
[+] Current address: T2 Biosystems, Cambridge MA 02141 (USA)

[**] Research and experiments were supported by the Director, Office of Science, Office of Basic Energy Sciences, Materials Sciences and Engineering Division, of the US Department of Energy under Contract No. DE-AC03-76SF00098. L.S. was supported by the Deutsche Forschungsgemeinschaft (SCHR 995/1-1) through an Emmy Noether Fellowship. T.J.L. acknowledges the Graduate Research and Education in Adaptive bio-Technology (GREAT) Training Program of the UC system wide Biotechnology Research and Education Program (#2005–264).

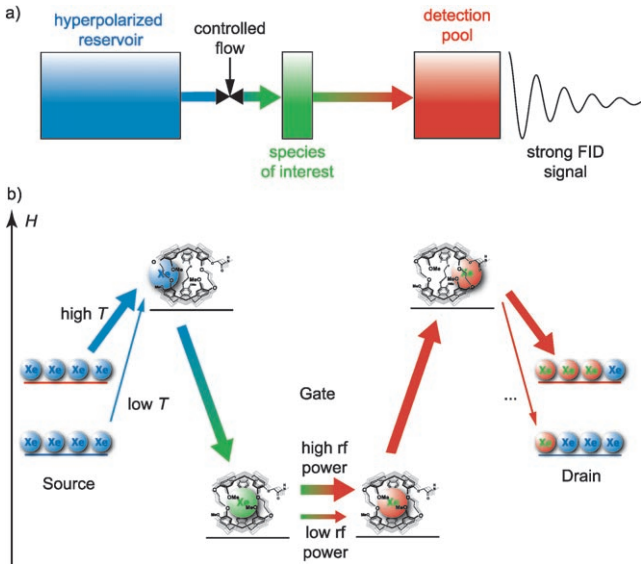

Figure 1. NMR signal enhancement through transfer of magnetization and its implementation for hp xenon atoms (transpletor concept). a) Magnetization transfer using a hp reservoir picks up information from a molecule of interest at low concentration. Controlling the flow from the reservoir allows gated transfer of the information into the detection pool. b) Flow diagram of hyperpolarized magnetization using a molecular host for controlled depolarization of ^{129}Xe guest atoms. Free hyperpolarized atoms (blue) represent the source of magnetization and can flow into the gate where they resonate at a different frequency (green) and can be saturated by a selective rf pulse. The depolarized nuclei (red) leave the cage and accumulate in the drain. Accessibility to the gate is determined by the activation barrier to enter the cage and can thus be controlled by temperature.

When using temperature to control depolarization transfer, three effects should be considered: First, increasing temperature increases the exchange rate of xenon with the cage molecules.[6,9,10] Second, the binding constant of the xenon–cage complex tends to increase as temperature increases,[11] making more xenon susceptible to selective saturation. Third, as the solubility of xenon in water decreases with increasing temperature up to ca. 310 K, the resulting smaller reservoir pool is easier to saturate.

However, temperature changes will only be of advantage if the significantly reduced residence time of the xenon inside the host will not cause a dramatic loss in saturation efficiency. The biosensor together with a selective rf pulse is expected to act in a similar fashion to a transistor. Figure 1 b illustrates the concept of this "transpletor" that transfers magnetization depletion by adjusting the flow of saturated xenon. Initially, the pool of free xenon atoms represents the source. Entering the host makes them sensitive to selective depolarization. The cage therefore represents the gate that must be passed to enter the pool of depolarized nuclei that corresponds to the drain. Changes of the flow into the drain contain combined information about changes in the exchange rate and the saturation efficiency. Ultimately, increasing the temperature should induce a stronger source-to-drain current.

This temperature-gated amplification was demonstrated by a set of signal depletion curves at different temperatures *T*. These curves show the decrease in bulk xenon magnetization

as a function of saturation time, t_{sat}. Herein, we used a biosensor that tracks avidin by its biotin moiety in aqueous solution.[12] Figure 2a shows the significant acceleration in reaching the maximum Hyper-CEST effect for the transition from 290 to 310 K. Using the function $I_{norm}(t_{sat}) = I_0 \exp(-t_{sat}/\tau)$ to model the data, the depolarization flow is proportional to the inverse of the time constant τ. Figure 2b demonstrates that τ^{-1} increases more than tenfold upon heating the sample by 20 K.

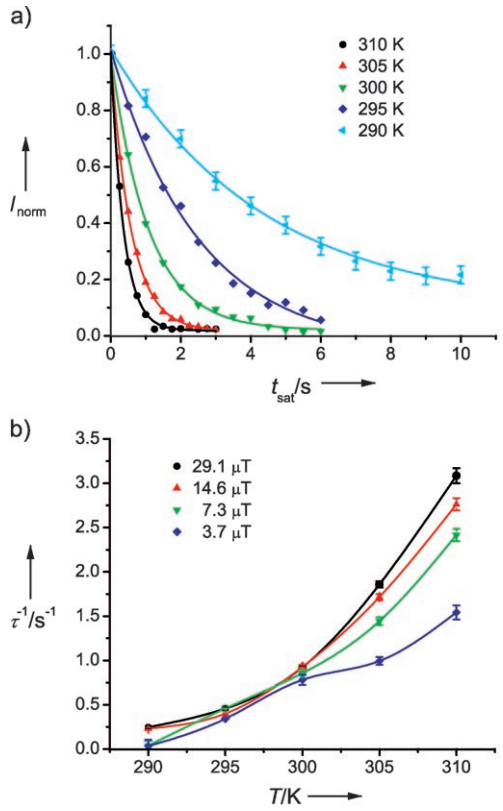

Figure 2. Source-to-drain depolarization flow control using Hyper-CEST with a cryptophane-A cage at different temperatures. a) Saturation curves for the normalized solution peak intensity, I_{norm}, of free dissolved ^{129}Xe in the presence of sensor with a concentration of 20 μM and saturation power $B_1 = 14.6$ μT at different temperatures. The time constant τ varies between 4.34 s for 290 K and 0.36 s for 310 K. b) Plot of τ^{-1} from saturation curves as in (a) as a function of temperature. Insufficient saturation occurs at high temperatures, as seen from the differences in τ^{-1} for different saturation powers. The pulse with $B_1 = 3.7$ μT has a bandwidth of $\Omega \approx 72$ Hz and is therefore only marginally wider than the resonance to be saturated at 310 K. Using the high power pulse ($B_1 = 29.1$ μT) with $\Omega \approx 614$ Hz ensures complete saturation even at high temperatures and reflects highly efficient transfer of depleted magnetization owing to increased xenon flow.

The problem of decreasing saturation efficiency is reflected by the observation that the increase of flow into the drain depends more on saturation power at higher temperatures. The shorter residence time causes homogenous line broadening which makes an rf pulse amplitude of $B_1 =$ 29.1 μT at 310 K almost twice as efficient as a pulse of 3.7 μT (Figure 2b). However, there is a temperature-gated amplification effect even for the low power pulse. This principle becomes relevant in two cases: First, the Hyper-CEST saturation power might be limited for rf safety reasons in biomedical imaging. Second, the use of low-bandwidth pulses is an important step for reading out different sensor signals in the same system (multiplexing).[7,10]

The transpletor concept was implemented with a biosensor imaging setup that uses a pulse sequence with a saturation bandwidth of only $\Omega \approx 30$ Hz (i.e., $B_1 = 1.6$ μT). This should yield ineffective saturation at $T \approx 300$ K but effective depletion transfer at slightly increased temperatures. ^{129}Xe MRI datasets were collected using a setup described in the Experimental Section. Figure 3a shows a coronal ^{1}H MR

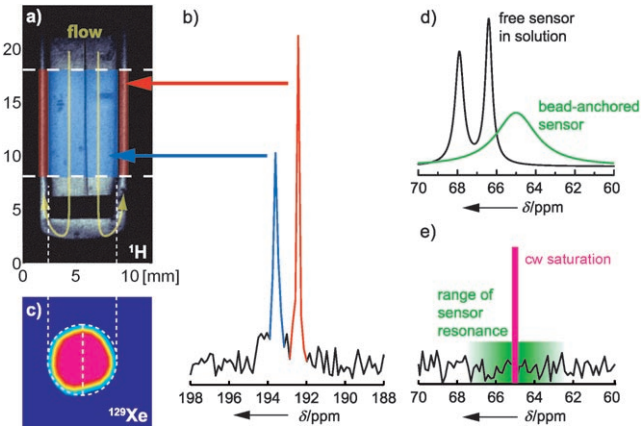

Figure 3. Conditions for ^{129}Xe MR imaging of functionalized cryptophane cages targeting microscopic beads. a) ^{1}H coronal image (12×24 mm^2 field of view) of the perfusion phantom showing the 10 mm transverse slice for xenon imaging (colored overlays). The center volume with the agarose beads is split in two compartments, only one of which contains the functionalized cryptophane-A cage. The agarose-filled part of the slice (blue) is the source of a resonance at $\delta = 193.6$ ppm, and the surrounding part of the outlet gap (red) is the source of a peak at $\delta = 192.5$ ppm. b) Single-shot slice-selective ^{129}Xe NMR spectrum showing the signals from the two colored regions in (a). c) Transverse ^{129}Xe image (12×12 mm^2 field of view) generated from the peak at $\delta = 193.6$ ppm showing distribution of the agarose beads. d) Lineform changes of the biosensor signal upon immobilization to microscopic structures such as agarose beads (schematic spectra with representative line widths reported in [9] and [8]) e) The biosensor resonance of ca. 210 Hz linewidth at $\delta = 65$ ppm (green box) is below the noise threshold (high-field part of the spectrum in (b)). However, low-power saturation with $B_1 = 1.6$ μT (corresponding to a saturation bandwidth of about 30 Hz; pink bar) will yield efficient saturation transfer at high temperature (see Figure 4).

image of the system with two samples of agarose beads, one sample labeled with the biosensor. The signal of xenon at $\delta =$ 193.6 ppm (aqueous solution with agarose) can be detected in a single-shot slice-selective spectrum (Figure 3b) and allows the spatial distribution of the microscopic beads to be displayed selectively (Figure 3c). In contrast, substantial line broadening (Figure 3d) and low concentration make the biosensor signal at $\delta \approx 65$ ppm undetectable without substantial signal averaging (Figure 3e).

Figure 4 illustrates the expected temperature-gated amplification for sensor detection. At 299 K, the Hyper-CEST

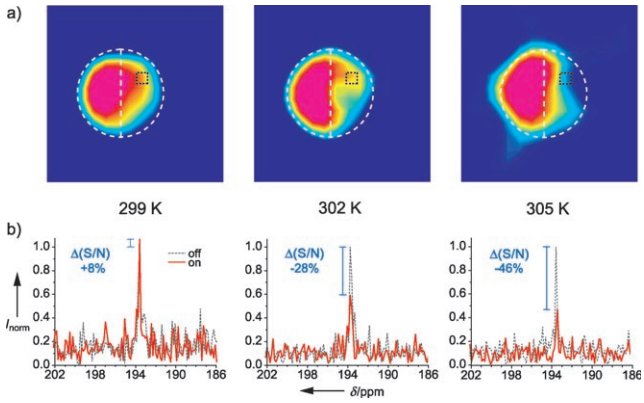

Figure 4. Application of the transpletor concept for temperature-sensitive molecular imaging. Compartments are indicated by white dotted lines. a) Transverse ^{129}Xe images show increasing contrast when the temperature is raised from 299 K to 305 K. The right compartment contains the biosensor with the functionalized cryptophane-A cage that responds only weakly to on-resonant saturation with $B_1 = 1.6\ \mu T$ for 1.5 s at 299 K. A higher temperature enhances the Hyper-CEST contrast and leads to significantly more efficient saturation. b) Corresponding spectra from the center of the right compartment (black dotted square) show the signal change for on-resonant saturation (red spectra; compared to black data for off-resonant saturation) at different temperatures. Whereas the S/N ratio is almost unchanged at 299 K, a signal decrease of 46% can be achieved after increasing the sample temperature by 6 K.

depletion is less effective, as demonstrated by the signal-to-noise (S/N) ratio in a spectrum from the sensor-labeled compartment: When comparing on-resonant with off-resonant saturation, the S/N ratio changes only by 8%, which is within the noise level. Increasing T by 3 K yields a change in the S/N ratio of −28%. Further heating to 305 K results in a significant rise in flow through the gate and consequently a 46% signal depletion, clearly emphasizing the sensor-free compartment on the left.

These data illustrate that, despite the reduced exposure time of nuclei to the cage environment, there is a significant increase in signal contrast at higher temperatures. Substantial line broadening of the bead-associated sensor (the resonance is over 200 Hz wide)[8] is not an issue in this case as inhomogeneous broadening, caused by immobilization, does not impede efficient saturation. Detecting structures of micrometer size becomes feasible with this technique, whereas conventional NMR readout fails to acquire even sufficient proton signal for localization of macromolecules.

In summary, we have demonstrated temperature-controlled molecular gates for optimized use of hp nuclei in liquid-state NMR spectroscopy. Biosensor detection now includes features of MRI thermometry[13]—which could be used to monitor hyperthermia in oncologic therapy[14]—but the concept of a transpletor also illustrates increased sensitivity at body temperature. Moreover, this concept can be applied to other problems that rely on exchangeable NMR-detected guests to reveal properties of the host structure or indirect detection of competing guests.[6,10,15,16] Such experiments would facilitate studies of the exchange dynamics of other nanostructure hosts (alternative cages, carbon nanotubes, zeolites).[17] In addition, both competing molecules (e.g. methanol or chloroform in solution) with comparable or higher binding constants and parameters that change the host accessibility of the hyperpolarized guest (e.g. solvation of xenon) will influence the flow of hyperpolarized nuclei through the gate, and could be detected with the transpletor. In this way, depolarization transfer enables sensitivity-enhanced detection of molecules even if they usually cannot directly benefit from hp techniques.

Experimental Section

Datasets were recorded on a 7.05 T NMR spectrometer (Varian, Palo Alto, CA) with a 10 mm probe. Hyperpolarized xenon ($P \approx 4.6\%$) was generated with a XenoSpin polarizer (Amersham Health, Durham, NC) using a mixture of 89% He, 10% N_2 and 1% nonenriched xenon (Isotec, Sigma Aldrich). For evaluating the signal depletion upon increasing saturation time at different temperatures, this mixture was bubbled for 25 s at 0.45 SLM (standard liters per minute) into an NMR tube containing ca. 2.5 mL of 20 μM biosensor solution. Gas flow was then interrupted using a stopped-flow system,[18] followed by a 5 s delay to wait for the disappearance of any bubbles. The Hyper-CEST experiment was then started with a variable cw-saturation delay and subsequent readout of a single 300 ms free induction decay (FID). The temperature of the system was controlled with the variable temperature unit of the spectrometer. After Fourier transformation (FT) and application of an apodization filter, the xenon solution signal at $\delta = 192.5$ ppm was integrated to determine signal depletion.

Imaging experiments were conducted with a gradient coil assembly (Resonance Research Inc., Billerica, MA) for spatial encoding. A two-compartment phantom described previously[8] contained avidin-labeled agarose beads (Immobilized Avidin, Pierce Biotechnology, Rockford, IL) and was perfused with water (6 mL min^{-1}) that was heated before entering the magnet with a 60 cm heating cable (5 W/30 cm power output; BH Thermal Corporation, Columbus, OH) and saturated with the polarizer gas mixture (0.65 SLM gas flow) immediately before entering the phantom.[19] One compartment contained the biosensor at 50 μM concentration. A thermocouple attached to the outlet channel of the phantom was used to read the temperature of the water directly after leaving the bead volume. The maximum achievable temperature of the water was 305 K owing to the need to keep the heating cable outside of the magnet and because of poor thermal conductivity of the tubing guiding the water.

^{129}Xe Hyper-CEST images were acquired using a 1.5 s cw-pulse of 1.6 μT amplitude and a slice-selective 90° pulse along the z dimension (2 ms, sinc shape, 10 mm slice thickness) with subsequent two-dimensional phase encoding (12×12 mm^2 field-of-view, matrix size 8×8 FIDs, 10.8 min acquisition time). Each point in k space was read out once for 64 ms with 100 kHz spectral width. Postprocessing using MATLAB (MathWorks, Inc., Natick, MA) included two-dimensional FT for spatial reconstruction after zero-filling to a 16×16 FIDs dataset and one-dimensional FT for spectral reconstruction. Images showing the spatial distribution of the bead signal at $\delta = 193.6$ ppm were generated by summation of the signal intensity over five data points ($\delta \approx 0.74$ ppm) in the absolute spectrum and subsequent color-encoding of these values.

Received: January 24, 2008
Published online: May 6, 2008

Keywords: biosensors · imaging agents · inclusion compounds · thermometry · xenon

[1] M. R. Bouchiat, T. R. Carver, C. M. Varnum, *Phys. Rev. Lett.* **1960**, *5*, 373 – 375.
[2] B. M. Goodson, *Concepts Magn. Reson.* **1999**, *11*, 203 – 223.
[3] C. R. Bowers, D. P. Weitekamp, *Phys. Rev. Lett.* **1986**, *57*, 2645 – 2648.
[4] D. Canet, C. Aroulanda, P. Mutzenhardt, S. Aime, R. Gobetto, F. Reineri, *Concepts Magn. Reson. Part A* **2006**, *28*, 321 – 330.
[5] D. A. Hall, D. C. Maus, G. J. Gerfen, S. J. Inati, L. R. Becerra, F. W. Dahlquist, R. G. Griffin, *Science* **1997**, *276*, 930 – 932.
[6] K. Bartik, M. Luhmer, J.-P. Dutasta, A. Collet, J. Reisse, *J. Am. Chem. Soc.* **1998**, *120*, 784 – 791.
[7] M. M. Spence, S. M. Rubin, I. E. Dimitrov, E. J. Ruiz, D. E. Wemmer, A. Pines, *Proc. Natl. Acad. Sci. USA* **2001**, *98*, 10654 – 10657.
[8] L. Schröder, T. J. Lowery, C. Hilty, D. E. Wemmer, A. Pines, *Science* **2006**, *314*, 446 – 449.
[9] T. J. Lowery, S. Garcia, L. Chavez, E. J. Ruiz, T. Wu, T. Brotin, J.-P. Dutasta, D. S. King, P. G. Schultz, A. Pines, D. E. Wemmer, *ChemBioChem* **2006**, *7*, 65 – 73.
[10] G. Huber, T. Brotin, L. Dubois, H. Desvaux, J.-P. Dutasta, P. Berthault, *J. Am. Chem. Soc.* **2006**, *128*, 6239 – 6246.
[11] P. A. Hill, Q. Wei, R. G. Eckenhoff, I. J. Dmochowski, *J. Am. Chem. Soc.* **2007**, *129*, 9262 – 9263.
[12] T. J. Lowery, S. M. Rubin, E. J. Ruiz, M. M. Spence, N. Winssinger, P. G. Schultz, A. Pines, D. E. Wemmer, *Magn. Reson. Imaging* **2003**, *21*, 1235 – 1239.
[13] S. Zhang, C. R. Malloy, D. A. Sherry, *J. Am. Chem. Soc.* **2005**, *127*, 17572 – 17573.
[14] C. Weidensteiner, B. Quesson, B. Caire-Gana, N. Kerioui, A. Rullier, H. Trillaud, C. T. Moonen, *Magn. Reson. Med.* **2003**, *50*, 322 – 330.
[15] L. Garel, B. Lozach, J.-P. Dutasta, A. Collet, *J. Am. Chem. Soc.* **1993**, *115*, 11652 – 11653.
[16] C. Garcia, D. Humilière, N. Riva, A. Collet, J.-P. Dutasta, *Org. Biomol. Chem.* **2003**, *1*, 2207 – 2216.
[17] C. J. Jameson, A. K. Jameson, R. Gerald II, A. de Dios, *J. Chem. Phys.* **1992**, *96*, 1676 – 1689.
[18] S.-I. Han, S. Garcia, T. J. Lowery, E. J. Ruiz, J. A. Seeley, L. Chavez, D. S. King, D. E. Wemmer, A. Pines, *Anal. Chem.* **2005**, *77*, 4008 – 4012.
[19] C. Hilty, T. J. Lowery, D. E. Wemmer, A. Pines, *Angew. Chem.* **2006**, *118*, 76 – 79; *Angew. Chem. Int. Ed.* **2006**, *45*, 70 – 73.

